ARL-MAT-REPORT-112

LEVEL

AR-001-756

DEPARTMENT OF DEFENCE

DEFENCE SCIENCE AND TECHNOLOGY ORGANISATION

AERONAUTICAL RESEARCH LABORATORIES

MELBOURNE, VICTORIA

MATERIALS REPORT 112

THE STRESS-WAVE RADIATION FROM GROWING CRACKS

by

L. R. F. ROSE

SEP 1 5 1980

Approved for Public Release.

© COMMONWEALTH OF AUSTRALIA 1979

AUGUST 1979

80 9   11 043

AR-001-756

DEPARTMENT OF DEFENCE
DEFENCE SCIENCE AND TECHNOLOGY ORGANISATION
AERONAUTICAL RESEARCH LABORATORIES

ARL/MAT—112

MATERIALS REPORT 112

THE STRESS-WAVE RADIATION FROM GROWING CRACKS.

by

L. R. F. ROSE

Aug 79

SUMMARY

Explicit formulae are given for the stress discontinuities radiated by a suddenly starting two-dimensional crack under tension, in an ideal elastic body. These formulae also give, with a change in sign, the stress discontinuities radiated by a suddenly stopping crack, and, with a geometrical deformation, those radiated by a three-dimensional crack. The stress in the primary radiation due to short crack-jumps is thus shown to vary in essentially the same manner as does the crack speed during the jump. The diffraction of the primary radiation from one tip of a centre-crack by the other tip produces a secondary radiation, whose properties depend mainly on the nature of the surface wave associated with the primary radiation. Since this first diffraction can lead to crack extension, further diffractions would be difficult to study analytically. If it is possible to isolate the primary radiation experimentally, however, it should give directly the essential characteristics of the source. This could be used to separate source-characteristics from specimen and transducer effects in acoustic emission studies of fatigue cracking, or stress-corrosion cracking.

DOCUMENT CONTROL DATA SHEET

Security classification of this page: Unclassified

1. Document Numbers	2. Security Classification
(a) AR Number: AR–001–756	(a) Complete document: Unclassified
(b) Document Series and Number: Materials Report 112	(b) Title in isolation: Unclassified
(c) Report Number: ARL–Mat–Report–112	(c) Summary in isolation: Unclassified

3. Title: THE STRESS-WAVE RADIATION FROM GROWING CRACKS

4. Personal Author: Rose, L. R. F.	5. Document Date: August, 1979
	6. Type of Report and Period Covered:

7. Corporate Author: Aeronautical Research Laboratories	8. Reference Numbers (a) Task: DST 76/92
9. Cost Code: 32-6720	(b) Sponsoring Agency:

10. Imprint: Aeronautical Research Laboratories, Melbourne	11. Computer Program(s) (Title(s) and language(s)):

12. Release Limitations (of the document)
Approved for Public Release

12-0. Overseas:	N.O.	P.R.	1	A	B	C	D	E	

13. Announcement Limitations (of the information on this page):
No Limitation

14. Descriptors: Elastic waves Cracking (fracturing) Nondestructive tests	15. Cosati Codes: 2001 2012 1402

16. *ABSTRACT*

Explicit formulae are given for the stress discontinuities radiated by a suddenly starting two-dimensional crack under tension, in an ideal elastic body. These formulae also give, with a change in sign, the stress discontinuities radiated by a suddenly stopping crack, and, with a geometrical deformation, those radiated by a three-dimensional crack. The stress in the primary radiation due to short crack-jumps is thus shown to vary in essentially the same manner as does the crack speed during the jump. The diffraction of the primary radiation from one tip of a centre-crack by the other tip produces a secondary radiation, whose properties depend mainly on the nature of the surface wave associated with the primary radiation. Since this first diffraction can lead to crack extension, further diffractions would be difficult to study analytically. If it is possible to isolate the primary radiation experimentally, however, it should give directly the essential characteristics of the source. This could be used to separate source-characteristics from specimen and transducer effects in acoustic emission studies of fatigue cracking, or stress-corrosion cracking.

CONTENTS

Accession For

NTIS GRA&I

DDC TAB

Unannounced

Justification

By

Distribution/

Availability Codes

Avail and/or

Dist   special

A

1. INTRODUCTION

The technique of non-destructive testing which relies on detecting the acoustic emission (or stress-wave emission) from a structure under load does not yet use all the information contained in the emission. This emission is usually detected by piezo-electric transducers attached to the structure, and the major aim of current research is to derive a more accurate interpretation of the recorded electrical signals, so as to improve upon the pragmatic approach which simply associates an increasing intensity of signals with a deterioration of the structure. In particular, this approach does not discriminate between the several sources of emission which may be active, although their respective emissions may in fact show different characteristics, and thus be separable (see, for example, [1]). We shall be concerned in this paper with the distinguishing features of the emission from growing cracks.

The basic theoretical result is that a sudden change in crack speed gives rise to stress discontinuities in the radiated body-waves. Explicit formulae for the discontinuities due to the sudden starting of a two-dimensional crack, under tension (Mode I), are given in section 2*. In section 3 we consider the surface wave on the crack faces due to the motion of one tip of a centre-crack, and the secondary radiation due to the diffraction of that wave by the other crack tip. A detailed derivation of the results given in sections 2 and 3 would be lengthy, but since it is not required for understanding these results, only the main steps are recorded here, in an appendix. The emphasis is placed instead on the proper use of the results in practice, for the theoretical models are, necessarily, very idealized.

In section 4 we show how Keller's geometrical theory of diffraction [3] can be used to derive the stress discontinuities radiated by three-dimensional cracks, starting from the two-dimensional results. Madariaga has recently performed an elaborate numerical analysis of the radiation from circular shear-cracks [4], and has subsequently shown [5] that the dominant features could be obtained quite simply from the relevant two-dimensional radiation patterns (modes II and III), by using Keller's theory; indeed, that approach led him to some sharper insights into his numerical results. This makes it unnecessary to undertake the laborious numerical calculations for the analogous tensile cracks.

The theoretical results given in section 2 pertain to the primary body-wave radiation. It would be difficult in practical applications to monitor only this primary radiation, but this can be done in laboratory experiments, if certain precautions are observed. It would be preferable to capture this radiation at normal incidence, since a simple model can then be used for determining the response of the piezo-electric transducer (section 5). We discuss in section 6 what the results of such an experiment are likely to be. Although we concentrate there on the longitudinal component of the radiation, it should be noted that the results given in earlier sections are based on exact solutions of the equations of elasticity, satisfying the proper boundary conditions on the crack faces (by contrast to [6], where these boundary conditions are not satisfied).

2. THE RADIATION FROM TWO-DIMENSIONAL CRACKS (Mode I)

The Starting Phase

Consider first the familiar two-dimensional idealization for a centre-cracked plate under tension (plane strain): the plate is assumed to be of infinite extent; the crack is taken to lie on the x-axis, say with crack tip A at $x = 0$, and tip B at $x = -l$; the stress at infinity reduces to a uni-axial tension σ parallel to the y-axis. The crack is open, but in equilibrium. The static stress intensity factor is given by $K_0 = \sigma(\pi l/2)^{\frac{1}{2}}$—see, for example, [7]. Now suppose that at

---

* Freund [2] discussed briefly the jump in average stress across the longitudinal wavefront, but there appears to be an error in the numerical results.

time $t = 0$ tip A begins to move with speed v. The radiation due to this motion will be called the *starting phase*, following [5]. The associated wavefronts are shown in Figure 1a, where we use the notation P for the longitudinal wave, S for the transverse wave, R for the surface (Rayleigh) wave, and SP for the head-wave. The stress discontinuities across the P- and S-wavefronts are most conveniently specified in terms of polar coordinates r, θ. Using $[\sigma_{rr}]_P$ to denote the jump in the normal stress σ_{rr} at the P-wavefront, we find (Appendix, §2) that

$$[\sigma_{rr}]_P = -\frac{(1 - \nu)K_0}{2(\pi r)^{\frac{1}{2}}} \frac{v}{c_L - v \cos \theta} \Omega(\theta), \tag{1}$$

$$\Omega(\theta) = \frac{\{(c_L/c_T)^2 - 2 \cos \theta\} (1 + \cos \theta)^{\frac{1}{2}}}{\{(c_L/c_R) + \cos \theta\} S (\cos \theta/c_L)}, \tag{2}$$

where c_L, c_T, c_R are the longitudinal, transverse and Rayleigh wavespeeds; ν is Poisson's ratio; and the function S involves an integral which has to be evaluated numerically (see Appendix, equation (A.4)). The following list of $S(\cos \theta/c_L)$, for values of $\cos \theta$ between 1 and -1, at intervals of $0 \cdot 2$, would enable the reader to reconstruct the plots in Figure 1b, with the help of only a pocket calculator: $0 \cdot 85, 0 \cdot 84, 0 \cdot 83, 0 \cdot 81, 0 \cdot 79, 0 \cdot 76, 0 \cdot 73, 0 \cdot 68, 0 \cdot 62, 0 \cdot 51, 0 \cdot 22$. These values, and all the numerical results given subsequently, hold for Poisson's ratio $\nu = 1/3$, which is a typical value for metals.

The important features of the result are:

(i) The strength of the discontinuity shows a decay proportional to $r^{-\frac{1}{2}}$, which is characteristic of cylindrical waves.

(ii) The angular dependence is best considered as the product of two factors: the first leads to a focussing of intensity directly ahead of the crack which becomes more pronounced for larger values of v; the second factor, $\Omega(\theta)$, is independent of v—it depends only on Poisson's ratio, and there is little variation for ν in the usual range of interest, $0 \cdot 2 \cdot \nu \cdot 0 \cdot 4$. Both factors are positive for $|\theta| < \pi$, with $\Omega \to 0$ as $\theta \to \pm \pi$. Thus, $[\sigma_{rr}]_P$ is negative. We also have $[\sigma_{\theta\theta}]_P = \{\nu/(1 - \nu)\} [\sigma_{rr}]_P$. The shear stress $\sigma_{r\theta}$, on the other hand, is continuous at the P-wavefront.

(iii) When the crack begins to grow, the stress intensity factor changes discontinuously from the value K_0 to the dynamic value $K_d = k(v)K_0$. The velocity factor $k(v)$, first derived by Freund [8], is approximately given by $k(v) = (1 - v/c_R) (1 - 0 \cdot 95v/c_T)$, ([9], p. 802). Thus, $[\sigma_{rr}]_P$ could have been related to the change in stress intensity factor $[K] = \{1 - k(v)\}K_0$, rather than to K_0, but this would have complicated the appearance of equation (1).

At the S-wavefront it is $\sigma_{r\theta}$ which is discontinuous, while the normal stress components σ_{rr}, $\sigma_{\theta\theta}$ are continuous. In the region $|\theta| < \cos^{-1}(-c_T/c_L) = \theta_c$, the jump in $\sigma_{r\theta}$ is given by (Appendix, §2)

$$[\sigma_{r\theta}]_S = -\frac{(1 - \nu)K_0}{4(\pi r)^{\frac{1}{2}}} \frac{v}{c_T - v \cos \theta} \Lambda(\theta), \tag{3}$$

$$\Lambda(\theta) = \frac{\sin 2\theta (c_T/c_L + \cos \theta)^{\frac{1}{2}}}{(c_T/c_R + \cos \theta) S (\cos \theta/c_T)}. \tag{4}$$

The angular factor $\Lambda(\theta)$ is positive for $|\theta| < \pi/2$, zero for $|\theta| = \pi/2$, and negative for $\pi/2 < |\theta| < \theta_c$.

In the region $|\theta| > \theta_c$, a head-wave (denoted by SP in Fig. 1a) precedes the S-wavefront. It contributes a logarithmic stress-discontinuity at the S-wavefront which may be derived from equations (A.10, 11). We shall not examine in detail the behaviour in this region, because it is usual in laboratory studies to monitor the acoustic emission ahead of the crack.

Figure 1b shows the relative magnitude of $[\sigma_{rr}]_P$ and $[\sigma_{r\theta}]_S$ (for $|\theta| < \theta_c$) when the crack speed $v = 0 \cdot 5 c_T$, with the normalization $(1 - \nu)K_0/\{2(\pi r)^{\frac{1}{2}}\} = 1$. The radiation patterns are symmetrical with respect to $y = 0$, so only one half of each is shown. The maximum value of $[\sigma_{r\theta}]_S$, which occurs at $\theta \simeq \pm 40°$, is less than one-fourth the maximum value of $[\sigma_{rr}]_P$, which occurs at $\theta \simeq \pm 85°$. The difference in the magnitude of these stress discontinuities is even more marked in the region $|\theta| < 30°$.

2

2.2 Short Crack-jumps

A *stopping phase* has the same pattern of wavefronts, and the stress discontinuity across these has the same angular variation as for a starting phase, but the opposite sign. This was shown to be the case for an anti-plane crack (mode III) by Eshelby [10]; it can be proved for the tensile case (mode I), as Madariaga [5] has done for shear cracks (mode II), on the basis of Kostrov's general solution for two-dimensional crack problems [11]. Thus, equations (1) and (3), without the first minus sign, also hold for a stopping phase, but v now denotes the crack's speed just before it stops, and K_0 must be replaced by a factor K^* which depends on the precise history of the crack's motion (cf. [12], §2). In practice one is often concerned with crack jumps which are much shorter than the current crack length, and it is then a reasonable approximation to take K^* equal to the static stress intensity factor for the current crack length.

There is no need to consider in detail what happens behind the wavefronts if one is only interested in short crack-jumps: for practical purposes, the variation of the compressive stress in the P-pulse (and of the shear stress in the S-pulse, ahead of the crack) is approximately the same as the variation in crack speed during the jump. For example, if the crack both starts and stops abruptly, the radiation ahead of the crack will consist of two approximately rectangular stress-pulses, whose duration will depend on the length of the jump, and whose amplitude will depend on K_0 and the crack speed v during the jump. It can be expected that in practice the pulses will not be that sharp, for at least two reasons: first, changes in crack speed are more likely to be only "effectively discontinuous", relative to an appropriate time-scale, rather than strictly discontinuous; and secondly, in the two-dimensional idealization all points on a straight crack-front move together, whereas in practice it is more likely that different portions of the crack front move at different speeds, and even at different times.

In spite of these smoothing effects, the body-wave radiation from growing cracks can still be expected to show "effective discontinuities" in stress, due to "relatively sudden" variations in crack speed, which occur typically when a crack begins to grow, or when a growing crack stops.

2.3 Correlation with the Stress Intensity Factor

The theoretical results for moving cracks show that the stress variation across a radiated wavefront is essentially the same as the variation of the stress intensity factor at the time of generation of the wave (cf. section 2.1 (iii)). This is also true for stationary cracks. For example, when a tensile load is suddenly applied to a centre-cracked plate, the stress intensity factor K increases in direct proportion with $t^{\frac{1}{2}}$, if the loading step-pulse strikes the crack at normal incidence at time $t = 0$. (K continues to increase until the diffracted wave from either tip reaches the other, when it begins to decrease, and then to oscillate about its eventual static value, [13].) It can be shown that now the radiated (or "diffracted") wavefronts, from the crack tip at $x = 0$, carry a change in stress which is initially proportional to $\tau^{\frac{1}{2}}$, if τ denotes the time elapsed since the arrival of the P- or S-wavefront at any given point (r, θ) ahead of the crack ($|\theta| < \pi/2$, $\tau = (t-r/c_L)$ or $(t-r/c_T)$ respectively). It is sufficient in fact to verify that this is the case for a semi-infinite crack, by starting from the results given in [14], §9.6.3.

Notice that in this case, with a stationary crack tip, K does not show a step-discontinuity, even though the incident pulse is discontinuous. It follows that if the starting phase, or the stopping phase, from one crack is diffracted by another neighbouring crack, the stress across the diffracted wavefronts will be continuous. Thus, stress discontinuities (or "effective discontinuities") are distinguishing features of the radiation from growing cracks.

3. THE DIFFRACTION OF THE STARTING PHASE

Figure 2 shows the displacement of the lower half of the crack surface when the P-wavefront of the starting phase from crack tip A has just reached tip B, which we suppose to have remained stationary. The only prominent feature is a small hump travelling to the left with speed c_R; even that is discernible only because we have assumed that tip A moves at the relatively high speed $v = 0 \cdot 5 c_L$ (see Appendix, §3).

The question now is to determine the variation ΔK_B of the stress intensity factor at B due to the diffraction of the starting phase. This will give as well the stress variation across the

diffracted wavefront radiated from B, according to the general result explained in section 2.3. The answer applies also to the case where both tips A and B start to move and stop shortly after, before the starting phase from either tip has reached the other. We find that

$$\Delta K_B(t) = -K_0 \int_{l/c_L}^{t} g(u)/(l/c_R - u)\, du, \qquad (5)$$

where $g(u)$ is a regular positive function (Appendix, §4). Thus, $\Delta K_B = 0$ until $t = l/c_L$, when the P-wavefront from A reaches B; it then takes a *negative* value, of gradually increasing magnitude, and tends logarithmically to a negatively-infinite value as t approaches l/c_R, the arrival time of the surface wave associated with the starting phase. This singular behaviour is due to the existence of a surface wave. Quite a different behaviour would be predicted for the corresponding anti-plane problem, where there is only one type of body-wave and no surface wave. There, the theoretical result is that $\Delta K_B = 0$ until $t = l/c_T$, and then it *increases* smoothly and monotonically—see (A.19).

With the tensile crack, the stress intensity factor at B falls to zero when $\Delta K_B = -K_0$ (*i.e.* before $t = l/c_R$). The crack is then effectively closed in the neighbourhood of B. The theoretical result is not valid beyond that time, for it would predict that the crack faces press against one another, whereas in its derivation it is supposed that this does not happen. However, this difficulty does not arise for the diffraction of a stopping phase, and the theoretical prediction then is that ΔK will increase logarithmically to a positively-infinite value. According to the theory of quasi-brittle fracture (see [7]), the crack will begin to extend at tip **B** if K_B exceeds the fracture toughness. It may stop shortly after, if the driving force is then below the critical value. Thus, a stopping phase from one tip can lead to a sequence of secondary radiation, due to the diffraction of successive stopping phases. This would be difficult to keep track of analytically.

The theoretical results, however, reflect the idealizations of the model. In addition to those discussed in section 2.2, there is the idealization that the crack faces are perfectly smooth: the surface wave then propagates unattenuated. In practice, the crack faces are rough, and will scatter the high-frequency component of the surface wave, converting it into body-wave radiation. We note also that the logarithmic approach to infinity is, in mathematical terms, less singular than the "inverse square-root" singularity reported by Freund [15] (see also [16], equation (35)) for the case where point-forces are suddenly applied to the faces of a crack. Freund [15] showed that the singularity is subdued, and virtually disappears, if the forces are applied gradually. One can expect a similar smoothing to occur if the crack accelerates gradually to the speed v, but the result in the present case cannot be obtained by a simple convolution: it requires a detailed tracking of the location of the crack tip at various retarded times (cf. [12], §4, for a similar anti-plane problem).

Although it is not possible, on purely theoretical grounds, to determine precisely what will happen in practice, it should be emphasized that the surface wave associated with the starting phase is not a theoretical artifact, but a real phenomenon. In particular, it is noted by Shmuely *et al.* [17] as being responsible for the seemingly premature crack-arrest observed for certain geometrical configurations, in their experiments.

4. THE RADIATION FROM A CIRCULAR CRACK

Suppose that at time $t = 0$ a circular crack appears on the plane $z = 0$, in a field of uniform tension parallel to the z-axis. The crack grows with constant speed v from zero-radius to a radius a, and then suddenly stops. For the purposes of illustration, it will be sufficient to consider only the longitudinal component of the radiation. The variation of stress immediately behind the spherical P-wavefront generated by the appearance of the crack is the same as it would be if the crack did not stop but continued to grow with speed v. It can be verified, from the known solution for the self-similar circular crack (see, for example, [18]), that the normal stress components are proportional to τ, the time elapsed since the arrival of the wavefront.

The dominant feature of the radiation, however, is the stress discontinuity carried by the stopping phase, as it is clearly shown by Madariaga's work for the analogous shear crack [5]. The manner in which this discontinuity is registered at any point may be derived from Keller's geometrical theory of diffraction [3] as follows. We imagine that each infinitesimal element of

4

the crack front generates, on stopping, a fan of rays in a plane normal to that element. With a circular front, only two of these rays pass through any given field-point Q: they come from that point on the front which is closest, and that which is furthest, from Q (Fig. 3). The ray from the closest point carries the step-discontinuity

$$[\sigma]_P = \frac{(1 - \nu) K}{2\{\pi R_1(1 + R_1/\rho_1)\}^{\frac{1}{2}}} \frac{v}{c_L - v \cos \beta} \Omega(\beta), \tag{6}$$

which is derived from the two-dimensional result given in equation (1) by making the following substitutions, using the notation shown in Figure 3:

(i) K_0 is replaced by K, which is approximately equal to the static stress intensity factor for a circular crack of radius a (cf. [5], §8);

(ii) θ is replaced by β;

(iii) $r^{-\frac{1}{2}}$ is replaced by $\{R_1(1 + R_1/\rho_1)\}^{-\frac{1}{2}}$, with $\rho_1 = a/\cos \beta$.

The last change is the most important one, and it amounts to a geometrical deformation to account for the curvature of the crack front. For large R, the amplitude of the discontinuity decays as R^{-1}, as it would for a spherical wave. The difference in sign between equations (1) and (6) is due to the fact that we are now considering a stopping phase. The stress component denoted by σ in (6) is the normal stress parallel to the ray; the discontinuity in the normal stress at right-angles to the ray is also given by (6) but with $(1 - \nu)$ replaced by ν (cf. the relation between σ_{rr} and $\sigma_{\theta\theta}$ in section 2.1). Since Keller's theory is valid asymptotically for high frequencies, it can be expected to give accurately the values of these step-discontinuities, and it is evident from Madariaga's work that this is indeed the case. The discontinuity carried by the ray from the furthest point is derived in a similar manner, but with θ replaced by $(\pi - \gamma)$. The delay between these two rays gives a useful measure of the effective width of the P-pulse of the primary radiation (except for $\alpha = \pi/2$, where there is a caustic). In the far field, i.e. for $R \gg a$, this delay is approximately equal to $(2a \cos \alpha/c_L)$.

The diffraction of the stopping phase will give rise to a secondary radiation, whose amplitude can again be derived on the basis of Keller's theory (because the symmetry of the present model implies that the energy redistributes itself uniformly, after the rays cross the caustic at the origin), but this will lead to the same problems of interpretation as were dealt with in the previous section. Also, the detailed calculations for the transverse component of the primary radiation will be complicated in the region where the head-wave precedes the S-wavefront.

The suddenly stopping circular crack may be considered as an idealized model for the fracture of brittle inclusions. Its most serious idealization is that the whole crack front stops simultaneously and suddenly. In practice, it is more likely that the fracture initiates near the inclusion/matrix interface, so that different portions of the crack front come to rest at different times. The implication here, as in sections 2 and 3, is that the radiation from the model has sharper features (viz. stress discontinuities), and a larger amplitude, than what is likely to be observed in practice. Nevertheless, the theoretical results can provide a useful guide in designing experiments and interpreting their results (see section 6).

5. THE RESPONSE OF A PIEZO-ELECTRIC TRANSDUCER TO A NORMALLY INCIDENT P-PULSE

There is a simple one-dimensional model for determining the response of a piezo-electric transducer to a normally incident, plane P-pulse. Although the model has been known for some time (see [19]), its potential usefulness appears to have been overlooked. It consists of an elastic slab, of uniform thickness d, sandwiched between two elastic half-spaces. The slab gives rise to a voltage proportional to the relative normal displacement of its faces; thus, the voltage is proportional to the integral of the normal strain, and also to the integral of the normal stress, across the thickness of the slab. The essential parameters are the acoustic impedances, which will be denoted by W_0 for the slab, W_1 for the half-space in which the pulse originates, and W_2 for the backing (to conform with the notation of [19], p. 116). In applying the model to a particular transducer, W_0 is taken to be equal to $\rho_0 c_0$, where ρ_0 is the density of the piezo-electric material, and c_0 is the speed of longitudinal waves across the thickness; the value for *PZT* 5A, which may be considered as typical, is $W_0 = 34$ (kg m^{-3} × km s^{-1})*.

---

* I am indebted to Mr I. G. Scott for supplying this information.

W_1 is the acoustic impedance of the specimen; for example, $W_1 = 17$ (kg m^{-3} × km s^{-1}) for aluminium. It is usually the case that the impedance W_2 of the backing material is less than W_1, so that there is reflection with a change of sign at the back interface. This leads to the characteristic ring-down of the recorded voltage in response to short pulses (see [19], Fig. 1.118, in which $W_0/W_2 = 9$).

To use the model we need its impulse response $I(t)$. This is not given in [19], but it is not difficult to show that it can be represented analytically by the following convolution product (denoted by an asterisk):

$$I(t) = kTf * \left\{ \sum_{n=0}^{\infty} (R_1 R_2)^n \delta [(c_0 t/2d) - n)] \right\},$$ (7)

$$T = 2W_0/(W_0 + W_1),$$

$$f(t) = \begin{cases} 1, & 0 < t < d/c_0, \\ R_2, & d/c_0 < t < 2d/c_0, \\ 0, & t < 0, \ t > 2d/c_0, \end{cases}$$

$$R_1 = (W_1 - W_0)/(W_0 + W_1), \ R_2 = (W_2 - W_0)/(W_0 + W_2).$$

δ denotes the Dirac delta-function. k denotes the dynamic piezo-electric constant; its actual value is not required for reconstructing the *shape* of the incident pulse. The step response $A(t)$, which is the integral of $I(t)$, is an oscillating function which approaches asymptotically the limiting value $kT(1 + R_2)/(1 - R_1 R_2)$, as shown in Figure 4. The response to a rectangular pulse of unit amplitude and duration Δt is $A(t) - A(t - \Delta t)$.

The model can be expected to give accurately only the initial response of a transducer, because the finite dimensions of the transducer, and the cross-coupling in piezo-electric materials, will play an increasingly important role in determining the response. Conversely, given an actual transducer output, one can expect to reconstruct accurately only the beginning of the stress pulse. But this is often sufficient to identify the source, as noted in [1], p. 98. Also, if the duration of the pulse is not much greater than the transit time d/c_0 (which is typically $0 \cdot 5\,\mu$s), one can expect to reconstruct the whole pulse accurately, and for this it is sufficient to retain only the first few terms of the series in equation (7). Figure 4 only required the first four terms; this should be sufficient in practice. The reconstruction involves a de-convolution which generally has to be performed numerically. This may be done directly in the time-domain (as in [1]), or in the frequency-domain, where de-convolution is equivalent to a division, by using the recently developed Fast Fourier Transform algorithm [20].

The experimental results shown in Figure 15 of [1] suggest that the model can in fact be useful for stress pulses of much longer duration than d/c_0. That figure shows the surface displacement as measured by a capacitive transducer, and the response of a piezo-electric transducer, due to a normally incident pulse. The overall shape of the displacement/time record is close to that of a ramp-function, with a rise-time of $30\,\mu$s; if it were precisely a ramp-function, the corresponding stress pulse would be rectangular and of $30\,\mu$s duration. The response of the piezo-electric transducer is in fact similar to that shown in our Figure 4; indeed, one can account for the finer details of the initial response by taking into account more precisely the actual stress variation.

It is important to note that the model assumes perfect acoustic contact between the transducer and the specimen. This is usually ensured in practice by applying a slight pressure to the transducer in attaching it to the surface. Also, it is not difficult to allow for the presence of a viscous couplant between the transducer and the specimen, within the framework of a one-dimensional model. The essential point is that while a proper modelling of the long-term response of a piezo-electric transducer would be complicated, its initial response to a normally incident pulse can be determined satisfactorily from a simple model. This can be used to advantage in designing experiments, as illustrated in the next section.

6. DISCUSSION

To simplify the discussion we shall consider a particular specimen, shown in Figure 5a, and

6

concentrate on the emission from one increment of crack growth. For example, with a fatigue crack, it would be convenient to isolate the emission produced by an increase in the maximum load for one cycle, after a steady-state has been reached under constant amplitude loading.

(There are differences of opinion on whether the acoustic emission from fatigue cracks is due mainly to crack growth or to dislocation sources (cf. [21, 22]), or even whether the crack growth occurs near the peak of the loading half of the cycle or during unloading (cf. [23, 24]). The point of view adopted here may be summarized as follows. Consider an actual compact tension specimen, and an ideally elastic model of it. Let the crack length in the model be adjusted according to the plastic-zone correction for small-scale yielding (see [7], §3.12; [25]). Then, during the early part of the overload cycle, the elastic stress field beyond a small region surrounding the crack tip will be the same in the specimen as in the model. To maintain the correspondence as the peak-load is approached, one must extend the crack in the model. What is not known in advance is the variation in crack speed during this extension which will give the best correspondence between the theoretical and the actual radiation. Once that is determined experimentally, one has a macroscopic characterization of the source which does not call into question the microscopic mechanisms of deformation and rupture which are responsible for the actual emission.)

In actual experiments, care should be taken to absorb as much as possible of the primary radiation when it reaches the edge of the specimen, especially the surface wave discussed in section 3 when it reaches the corners C in Figure 5a, at least until the primary radiation is well understood. We suppose that the experiment is set up to record this primary radiation, say at an angle of $30°$ to the direction of the crack. The specimen in Figure 5a is a compact tension specimen (like that used in [22]), but with one corner cut off so that the transducer at location A receives the radiation at normal incidence. The specimen is supposed to be sufficiently thick to accommodate fully that transducer.

The normal stress σ_{rr} carried by the P-pulse can now be reconstructed from the response of a piezo-electric transducer at A, by using the model of section 5, or the corresponding normal surface displacement at A can be monitored by using a capacitive transducer, as in [1]. In either case, the properties of the P-pulse should be sufficient to characterize the source, for short crack-jumps (cf. section 2.2).

The transducer at B is placed, as usual, on one of the broad faces of the specimen, say the face lying in the plane $z = h$, the other face lying in the plane $z = -h$. It would be difficult to predict the response at B, and what follows is only a qualitative discussion of what can be expected there if the P-pulse registered at A is a narrow rectangular pulse, approaching an impulse. The first difficulty is that the results of section 2 are valid only if a state of plane strain prevails throughout the specimen, but this is not the case on the faces $z = \pm h$. The most important modification which must be made is to cancel the stress σ_{zz} ($= \nu(\sigma_{rr} + \sigma_{\theta\theta})$), predicted by the plane-strain solution, over an expanding quasi-annular region, representing the intersection of the two-dimensional circular wavefronts of the P-pulse with the surfaces $z = \pm h$. The expected normal displacement u_z on $z = h$ shown in Figure 5b was obtained by smoothing the singularities of the theoretical solution for u_z due to an expanding circular ring-load on a half-space [26], but retaining a sense of the relative magnitudes of the various components of this surface "bulge". It is not called a surface wave because the leading edge clearly travels with the speed of longitudinal waves, which, in metals, is approximately twice the speed c_R of surface waves. On the other hand, it is also clear from Figure 5b that the major hump does travel with speed c_R, and it can properly be called a surface wave: in particular, there would be the characteristic retrograde-elliptical particle motion associated with that hump (cf. [14], §5.11). The response of a piezo-electric transducer at B will depend critically on the manner in which it is attached to the surface, for example on whether it is perfectly bonded to the surface, or kept at a certain distance from it due to the use of a couplant. Whatever the precise conditions may be, we can anticipate that:

(i) the apparent duration of the pulse will depend on the size of the transducer, being longer for a larger transducer;

(ii) unlike the P-pulse, the surface bulge will not be narrow, and indeed its width will increase with distance from the source, since the leading edge travels faster than the surface wave component;

(iii) in using the theoretical solution for a ring-load on a half-space, we have ignored the

7

reflections back and forth between the faces $z = \pm h$, which will further contribute to the apparent broadening of the pulse; and

(iv) if B is sufficiently far from the crack tip, the body-waves generated by cancelling σ_{zz} on $z = -h$ will reach B before the surface wave travelling on $z = h$.

These comments also apply to the response of a capacitive transducer at B.

The crux of the discussion is this: with the transducer at A we are dealing with an essentially two-dimensional situation; with the transducer at B we are inextricably in a difficult three-dimensional situation. Although in the practical application of acoustic emission monitoring the transducer will generally be in location B, in laboratory experiments an additional transducer can be used in location A. This should allow one to reconstruct the P-pulse of the primary body-wave radiation, which should characterize the source and thus provide a secure basis for the interpretation of the signals registered at B. In particular, this could be used to separate source-characteristics from specimen and transducer effects in acoustic emission studies of fatigue cracking, or stress-corrosion cracking.

APPENDIX

1. Introduction. Notation

The problems to be considered below are solved by integral transform methods: the basic techniques are explained in [14], chapters 7 and 9; the major innovation required here is due to Kostrov [11]. We shall adopt the notation used in our previous work [16], subsequently referred to as I. In particular, a circumflex is used to denote a Laplace transform over time, with parameter s, and the corresponding capital letter is used when the transformation over time is followed by a bilateral Laplace transformation over x, with parameter $s\chi$. a, b, c, d denote the reciprocals $1/c_L$, $1/c_T$, $1/c_R$, $1/v$; λ, μ the Lamé constants. The crack problems may be reduced to mixed boundary-value problems for a half-space ($y \geqslant 0$), and the condition of symmetry ($\sigma_{zy}(y=0)=0$) leads to the relation (I: (7))

$$U_y(\chi, o, s) = -\kappa \{M(\chi)/s\} \, \Sigma_{yy}(\chi, o, s) \,, \tag{A.1}$$

$$\kappa = (1 - \nu)/\mu \,, \tag{A.2}$$

on the boundary ($y = 0$) of the half-space. In the solution of crack problems it is necessary to factorize the kernel $M(\chi)$ as follows (I, §4):

$$M = M^+ . M^-, \quad M^-(\chi) = M^+(-\chi) \,,$$

$$M^+(\chi) = (a + \chi)^{\frac{1}{2}}/\{(c + \chi)\, S(\chi)\} \,, \tag{A.3}$$

$$S(\chi) = \exp\left[-\frac{1}{\pi} \int_a^b \arctan\left\{ \frac{4u^2 (u^2 - a^2)^{\frac{1}{2}} (b^2 - u^2)^{\frac{1}{2}}}{(2u^2 - b^2)^2} \right\} \frac{du}{u + \chi} \right]. \tag{A.4}$$

A supercript + attached to a function of χ indicates that the function is "analytic to the right", and consequently its inverse is identically zero for $x < 0$.

2. The starting phase

The appropriate boundary conditions are:

$$\sigma_{yy}(o < x < vt, o, t \geqslant o) = -K_0/(2\pi x)^{\frac{1}{2}} \,,$$

$$\sigma_{yy}(x < o, o, t) = 0 \,,$$

$$u_y(x > vt, o, t) = 0 \,.$$

Notice that we are using only the singular part of the prior static field ahead of the crack: this simplifies considerably the expression for the dynamic stress field generated by the motion (cf. the discussion of the static factor K^* in [12], §2), but it gives accurately the stress step-discontinuities at the wavefronts.

The main steps are the following:

(i) First, the double transform of Kostrov's pseudo-stress $P(\chi, s)$, defined in I: (52), is derived. This proves to be the same as the double transform of the actual stress for the corresponding anti-plane problem (cf. [5], §4).

(ii) From this we find the double transform of the actual stress on $y = 0$ to be

$$\Sigma_{yy}(\chi, o, s) = P(\chi, s)/\{(b + \chi)^{\frac{1}{2}} M^+(\chi)\}, \quad \text{(by definition)},$$

$$= -K_0/\{\sqrt{2}\, s^{3\,2}(d + \chi)\, M^+(\chi)\} \,. \tag{A.5}$$

(iii) Using the equations

$$s^2 \, \Phi(\chi, o, s) = -(\kappa/b^2)\,(\gamma/\alpha)\, M\Sigma_{yy}(\chi, o, s) \,, \tag{A.6}$$

$$\Psi(\chi, o, s) = -(2\chi\alpha/\gamma)\,\Phi(\chi, o, s)\,, \tag{A.7}$$

(where α denotes a branch of $(a^2 - \chi^2)^{\frac{1}{2}}$ with positive real part, $\gamma = (2\chi^2 - b^2)$, cf. I: (6)), we can derive the double transforms of the displacement potentials ϕ, ψ and proceed to perform their inversion by the Cagniard—de Hoop technique ([14], §7.9). With the notation

$$\zeta = -(t/r)\cos\theta + i\{(t/r)^2 - a^2\}^{\frac{1}{2}}\sin\theta\,,$$

where ζ is the value of χ along the Cagniard contour in the upper half-plane, and (r, θ) are the polar coordinates of the point (x, y), we have

$$\zeta_{,t} = i(a^2 - \zeta^2)^{\frac{1}{2}}/(t^2 - a^2 r^2)^{\frac{1}{2}}\,,$$

$$Im\,[\Phi\chi_{,t}]_{\chi=\zeta} = (t^2 - a^2 r^2)^{\frac{1}{2}}\,Re\,[\alpha\Phi]_{\chi=\zeta}\,,$$

so that the inversion integral with respect to $s\chi$ is brought into the form

$$\phi(r, \theta, s) = s^{-5/2}\,(A/\pi)\int_{ar}^{\infty}\frac{f(r, \theta, t)}{(t^2 - a^2 r^2)^{\frac{1}{2}}}\,e^{-st}\,dt\,, \tag{A.8}$$

where $A = (\kappa/b^2)\,(K_0/\sqrt{2})$, and $f(r, \theta, t)$ is the value of $Re\,[s^{5/2}\,\alpha\Phi/A]$ along the Cagniard contour $\chi = \zeta$. A similar expression can be derived for $\psi(r, \theta, s)$ in the region $|\theta| < \theta_c$.

(iv) The inversion with respect to s now proceeds by using the convolution theorem. It is more convenient to carry out this inversion for the time derivatives $\phi_{,tt}, \psi_{,tt}$, because these show directly the stress variation at the wavefront (see below). We find that

$$\phi_{,tt}(r, \theta, t) = A\pi^{-3/2}\int_{ar}^{t}\frac{f(r, \theta, u)}{(u^2 - a^2 r^2)^{\frac{1}{2}}}\,\frac{du}{(t - u)^{\frac{1}{2}}}\,,$$

so that, by virtue of the result

$$\int_{0}^{\tau}\{u(\tau - u)\}^{-\frac{1}{2}}\,du = \pi$$

which holds for all τ, and in particular for $\tau \to 0_+$, $\phi_{,tt}$ is found to have a step-discontinuity at the P-wavefront, given by

$$[\phi_{,tt}]_P = \{A/(2\pi ar)^{\frac{1}{2}}\}f(r, \theta, ar)\,. \tag{A.9}$$

It will be noticed that $f(r, \theta, ar)$, which gives the angular variation of the discontinuity, is in fact equal to

$$Re\,[s^{5/2}\,\alpha\Phi/A] = Re\,[\gamma M^-(\chi)/(d + \chi)]\,,$$

evaluated at the point $\chi = a\cos\theta$ where the Cagniard contour intersects the real axis. This angular variation is the same as that given in equations (1) and (2) of the main text.

(v) The inversion for $\psi_{,tt}$ proceeds in the same manner for $|\theta| < \theta_c$, but for $|\theta| > \theta_c$ the Cagniard contour must be deformed around a branch cut on the real axis (cf. [14], Fig. 7.12). The angular variation of the discontinuity in $\psi_{,tt}$ across the circular part of the S-wavefront is then obtained by evaluating $Re\,[s^2\beta\Psi]$ at the point where the Cagniard contour meets the branch cut in the upper half-plane (β denotes a branch of $(b^2 - \chi^2)^{\frac{1}{2}}$ with positive real part). Also, the part of the inversion contour around the branch cut gives rise to a head-wave, which precedes the S-wavefront, and it contributes a logarithmic discontinuity given by

$$-\frac{(1 - \nu)K_0}{4\pi\mu\,(\pi r)^{\frac{1}{2}}}\,\frac{v}{1 - bv\cos\theta}\,L(\theta)\log|t - br|\,, \tag{A.10}$$

$$L(\theta) = \{\sin 2\theta\,(a/b + \cos\theta)^{\frac{1}{2}}/(c + b\cos\theta)\}\,Im\,[1/S\,(b\cos\theta)]\,. \tag{A.11}$$

(vi) The stress discontinuities can now be derived from the relations between the stress components and the displacement potentials ([14], §3.13), by using the operator identity $\partial/\partial r = -(1/c)\,\partial/\partial t$, which holds at the wavefronts ([14], §4.5.3; $c = c_L$, c_T at the P and S-wavefronts respectively). Thus, for the normal stress σ_{rr} at the P-wavefront, we have

$$\sigma_{rr} = (\lambda + 2\mu)\,a^2\phi_{,tt} - (\lambda a/r)\,\phi_{,t} + r^{-2}\,\phi_{,\theta\theta},$$

since $\psi = 0$ before the S-wavefront arrives. In view of the wavefront expansion given for $\phi_{,tt}$ in (A.9), it is clear that the wavefront behaviour of σ_{rr} is dominated by the step-discontinuity in the term $(\lambda + 2\mu)\,a^2\,\phi_{,tt}$. This leads to the result given in equations (1) and (2) of the main text. The behaviour of the other stress components is deduced by similar considerations.

3. Displacement of the crack faces

From (A.1) and (A.5) we have

$$U_y(\chi, o, s) = s^{-5/2}\,CM^-(\chi)/(d + \chi), \tag{A.12}$$

with $C = \kappa K_0/\sqrt{2}$. The inversion with respect to $s\chi$ is easily carried out for $x > 0$: the inversion contour can be closed to the left, and the value of the integral is simply the residue at $\chi = -d$. Thus,

$$\hat{u}_y(x, o, s) = s^{-3/2}\,CM^-(-d)\,e^{-sdx},$$

and hence, by using the convolution theorem for the inversion over s, we find

$$u_y(x > o, o, t) = 2\pi^{-1}\,CM^+(d)\,(t - xd)^{\frac{1}{2}}, \quad xd < t, \tag{A.13}$$

sine $M^-(-d) = M^+(d)$.

The inversion for $x < 0$ is more complicated: the inversion contour is deformed to the right onto the branch cut, and the resulting integral has to be evaluated numerically. This is not easy because of the term S in the kernel (cf. (A.3), (A.4)). One can use a rational approximation for S (e.g. [13], Appendix), but we have preferred instead to use the approximation introduced in 1; this leads to an inversion in closed form. The idea is to replace (A.3) by

$$M^+(\chi) = (h + \chi)^{\frac{1}{2}}/(c + \chi). \tag{A.14}$$

The best choice for h is discussed in 1: for practical purposes one can take $h = 0.95b$. When the inversion contour is deformed on to the branch cut we now obtain

$$\hat{u}_y(x < o, o, s) = s^{-3/2}\,(C/\pi) \int_h^{\infty} \frac{(\xi - h)^{\frac{1}{2}}}{(d + \xi)(\xi - c)}\,e^{s\xi x}\,d\xi.$$

The inversion over s leads to

$$u_y(x < o, o, t) = 2C\,(|x|/\pi)^{\frac{1}{2}}\,F,$$

where F is a convolution integral which can be evaluated in closed form by turning it into a contour integral around a closed loop L surrounding a branch cut between $h\,|x|$ and t:

$$F = \frac{1}{2\pi i} \oint_L \frac{\{(t - \zeta)(h\,|x| - \zeta)\}^{\frac{1}{2}}}{(\zeta + |x|d)(\zeta - c|x|)}\,d\zeta.$$

If the loop is deformed into a circle about the origin of radius $r \to \infty$, the value of the integral can be derived from the residues at $c|x|$, $-|x|d$, ∞, when $t < c|x|$. For $t > c\,|x|$ the pole at $\zeta = c|x|$ is not crossed in the process of deforming the contour of integration: the residues at $-|x|d$ and ∞ then lead to the Cauchy principal value of F. We thus find, with

$$R_c = (c - h)^{\frac{1}{2}}\,(c|x| - t)^{\frac{1}{2}}/\{(c + d)\,|x|^{\frac{1}{2}}\},$$

$$R_d = (h + d)^{\frac{1}{2}}\,(t + |x|d)^{\frac{1}{2}}/\{(c + d)\,|x|^{\frac{1}{2}}\},$$

$$R_\infty = -1,$$

that

$$u_y(-t/c < x < o, o, t) = 2C (|x|/\pi)^{\frac{1}{2}} (R_c + R_d + R_\infty),$$ (A.15)

$$u_y(-t/h < x < -t/c, o, t) = 2C (|x|/\pi)^{\frac{1}{2}} (R_d + R_\infty).$$ (A.16)

Now, to determine the actual displacement of the crack faces, we must add the displacement given by (A.13, A.15, A.16) to the prior static crack opening, given by (see [7])

$$u_y(-l < x < o, o, t < 0) = \{\sigma(1 - \nu)/\mu\} \{-x (l + x)\}^{\frac{1}{2}}.$$

(Note that $2C = \sigma(\pi l)^{\frac{1}{2}} (1 - \nu)/\mu$).

4. The diffraction of the starting phase

To study this problem it is more convenient to suppose that it is the crack tip at $x = 0$ which remains stationary, and the one at $x = -l$ which moves to the left with speed v. From I: (30) we have

$$\Delta K (s) = -\sqrt{2} \int_0^\infty \sigma_{yy}(-u, s) \, \hat{m}^+ (u, s) \, du.$$

Using the formula for the Laplace transform of a product, and equation (A.5) for Σ_{yy} (allowing for a shift of origin), we obtain

$$s (\Delta K/K_0) = \frac{1}{2\pi i} \int_B \frac{M^+(-\chi) \, e^{-l s x}}{(d + \chi) \, M^+(\chi)} \, dx.$$

The inversion contour B is deformed to the right on to the branch cut to give

$$s (\Delta K/K_0) = \frac{1}{\pi} \int_a^\infty \frac{Im \, [M^-(\xi)]}{(d + \xi) \, M^+(\xi)} \, e^{-sl\xi} \, d\xi,$$

and the inversion over s then leads to

$$\Delta K (t \geqslant al) = \frac{K_0}{\pi} \int_{al}^t \frac{Im \, [M^-(u/l)]}{(u + ld) \, M^+(u/l)} \, du.$$ (A.17)

The essential feature is a pole in the integrand; it is more clearly evident if we use the approximate kernel (A.14), which gives

$$\Delta K (t \geqslant hl) = -\frac{K_0}{\pi} \int_{hl}^t \left(\frac{u + lc}{u + ld}\right) \left(\frac{u - hl}{u + hl}\right)^{\frac{1}{2}} \frac{du}{lc - u}.$$ (A.18)

For the corresponding anti-plane problem we can similarly derive the result

$$\Delta K (t \geqslant bl) = \frac{K_0}{\pi} \int_{bl}^t (u + ld)^{-1} \left(\frac{u + bl}{u - bl}\right)^{\frac{1}{2}} \, du.$$ (A.19)

REFERENCES

[1] N. N. Hsu and S. C. Hardy, in *Elastic Waves and Non-destructive Testing of Materials*, Y. H. Pao (ed.), AMD, Vol. 29, ASME (1978).

[2] L. B. Freund, *Journal of Applied Mechanics*, 39 (1972), pp. 601–602.

[3] J. B. Keller, in *Calculus of Variations and its Applications, Symposia on Applied Mathematics*, Vol. 8, McGraw-Hill (1958).

[4] R. Madariaga, *Bulletin of the Seismological Society of America*, 66 (1976), pp. 639–666.

[5] R. Madariaga, *Geophysical Journal of the Royal Astronomical Society* 51 (1977), pp. 625–651.

[6] K. Malen and L. Bolin, *Physica Status Solidi* (b), 61 (1974), pp. 637–645.

[7] J. F. Knott, *Fracture Mechanics*, Chapter 3, Butterworths (1973).

[8] L. B. Freund, *Journal of Mechanics and Physics of Solids*, 20 (1972), pp. 129–140.

[9] L. R. F. Rose, *International Journal of Fracture*, 12 (1976), pp. 799–813.

[10] J. D. Eshelby, *Journal of Mechanics and Physics of Solids*, 17 (1969), pp. 177–199.

[11] B. V. Kostrov, *International Journal of Fracture*, 11 (1975), pp. 47–56.

[12] L. R. F. Rose, *International Journal of Fracture*, 12 (1976), pp. 829–841.

[13] S. A. Thau and T. H. Lu, *International Journal of Solids and Structures*, 7 (1971), pp. 731–750.

[14] J. D. Achenbach, *Wave Propagation in Elastic Solids*, North-Holland (1973).

[15] L. B. Freund, *International Journal of Engineering Science*, 12 (1974), pp. 179–189.

[16] L. R. F. Rose, *Proceedings of the Royal Society of London*, A 349 (1976), pp. 497–521.

[17] M. Shmuely, D. Peretz and M. Perl, *International Journal of Fracture*, 14 (1978), R69–R72.

[18] J. R. Willis, *Philosophical Transactions of the Royal Society of London*, 274 (1973), pp. 435–491.

[19] J. Krautkramer and H. Krautkramer, *Ultrasonic Testing of Materials*, §1.103, Springer-Verlag (1969).

[20] E. O. Brigham, *The Fast Fourier Transform*, Prentice-Hall (1974).

[21] L. J. Graham and G. A. Alers, in *Monitoring Structural Integrity by Acoustic Emission*, ASTM, STP 571 (1975).

[22] T. C. Lindley, I. G. Palmer and C. E. Richards, *Materials Science and Engineering*, 32 (1978), pp. 1–15.

[23] R. J. H. Wanhill, *Metallurgical Transactions*, 6 A (1975), pp. 1587–1596.

[24] C. Laird, *Metallurgical Transactions*, 8 A (1977), pp. 657–664.

[25] T. M. Edmunds and J. R. Willis, *Journal of Mechanics and Physics of Solids*, 25 (1977), pp. 423–455.

[26] D. C. Gahkenheimer, *Journal of Applied Mechanics*, 38 (1971), pp. 99–110.
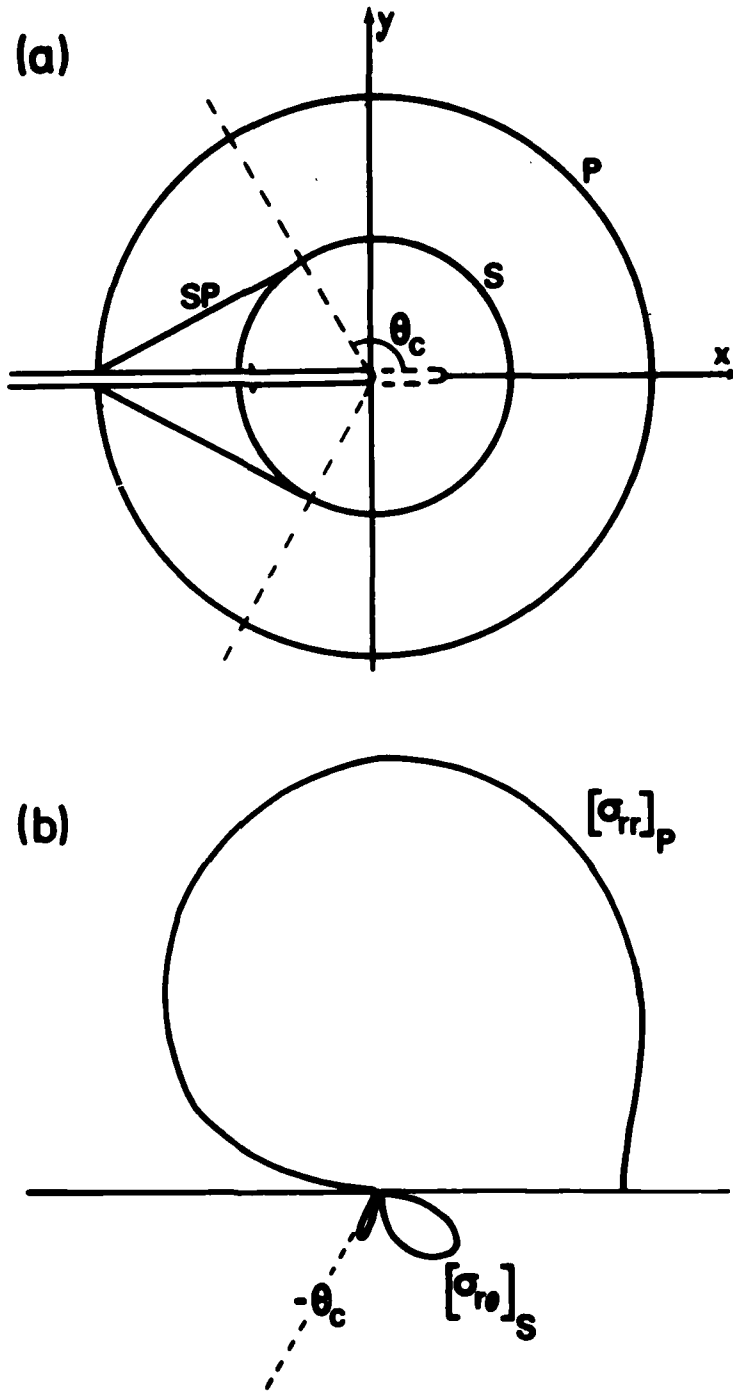
Fig. 1 : (a) The pattern of wavefronts associated with the starting phase.
(b) Radial plots of the step-discontinuity in σ_{rr} at the P-wavefront (top), and in $\sigma_{r\theta}$ at the S-wavefront (bottom), for $v = 0.5\, c_T$ and $v = 1/3$.

Fig. 2 : The displacement of the lower half of the crack surface, $u^o_y = u_y (x, y \to 0\text{-}, \ t = l/c_L)$. The dashed curve shows the initial crack opening. A' is the current position of tip A. The depth of the crack relative to its length was determined by setting $\sigma(1-\nu)/2\mu = 1$.
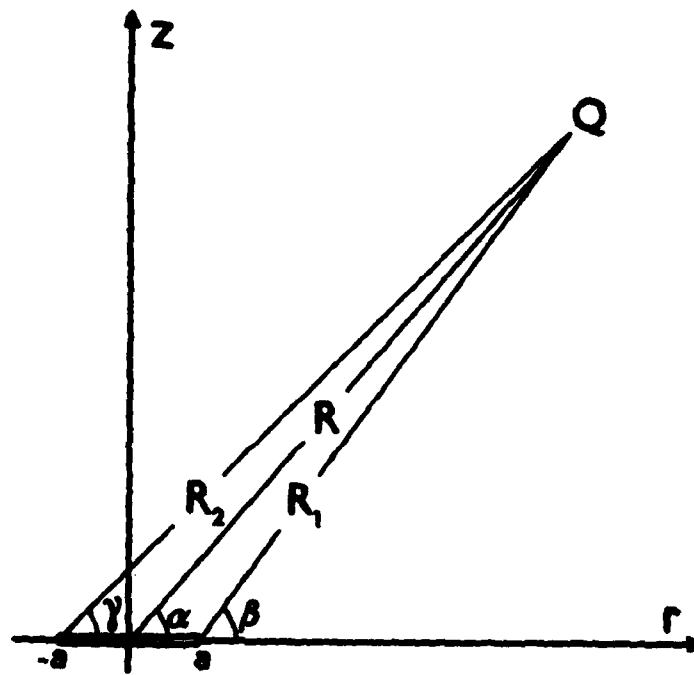
Fig. 3: Co-ordinates and notation for the radiation from a circular crack. $r = (x^2 + y^2)^{1/2}$.
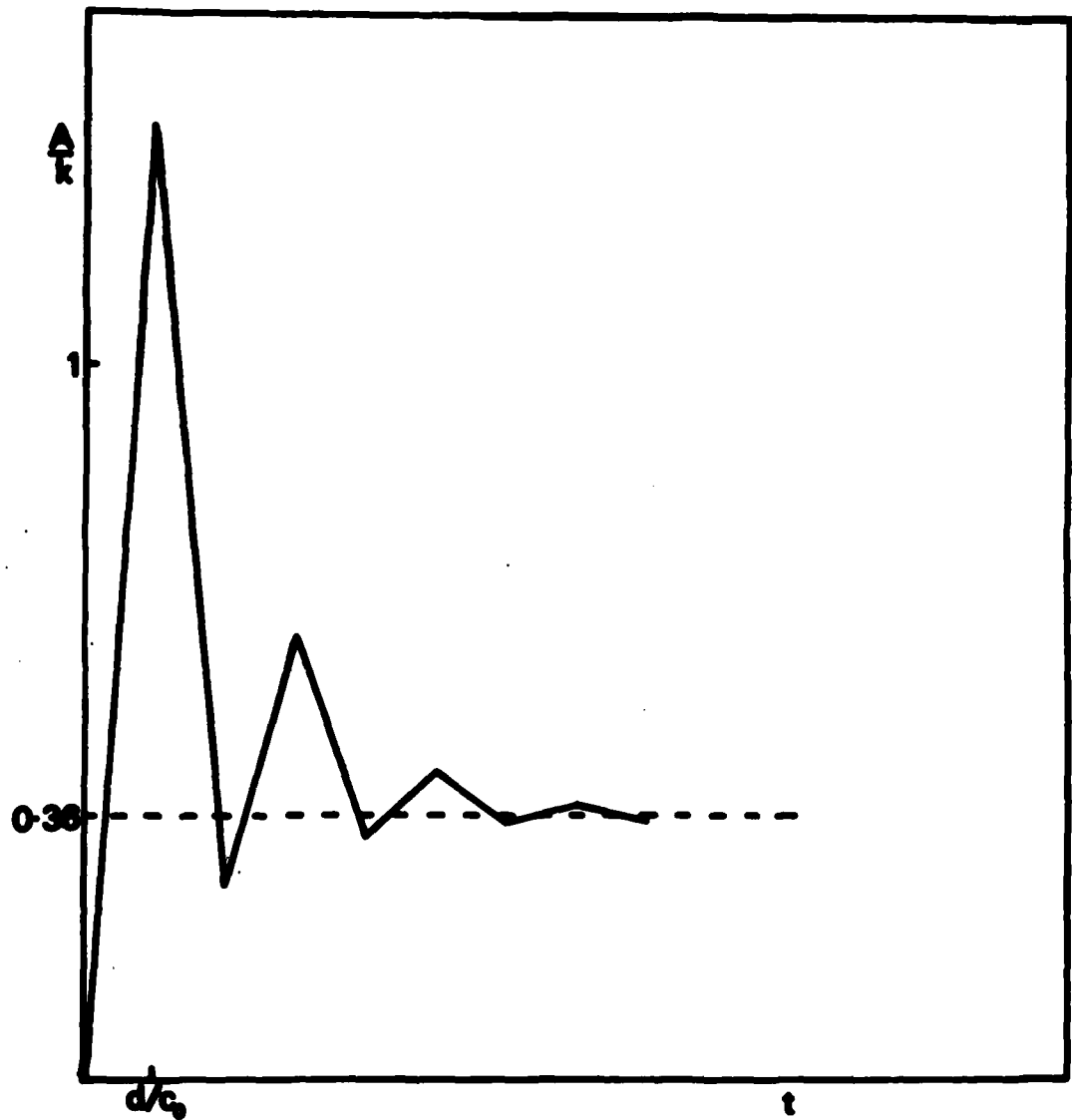
Fig. 4: The step response A(t) for the model of a piezo-electric transducer, with $W_0/W_1 = 2$, $W_0/W_2 = 9$.

(a)

(b)
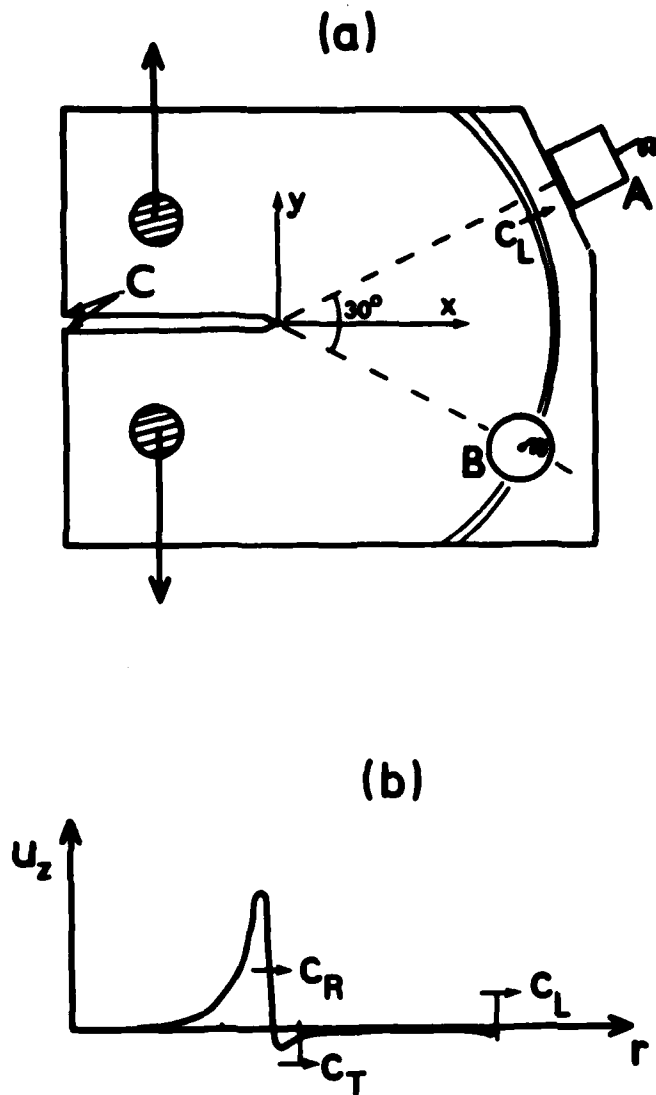
Fig. 5 : (a) The specimen considered in Sectior. 6, showing the location of transducers A and B. (b) A schematic representation of the normal surface displacement along a radial line ($\theta = 30°$) on $z = h$, when a narrow rectangular P-pulse is radiated by the crack.

DISTRIBUTION